JOURNAL OF SOLID STATE CHEMISTRY 135, 260–268 (1998)
ARTICLE NO. SC977632

Perovskite-Related Phases in the $Sr_4Nb_4O_{14}$–$Sr_5Nb_4O_{15}$–$SrTiO_3$ System

D. Pasero and R. J. D. Tilley

School of Engineering, University of Cardiff, P.O. Box 685, Cardiff CF2 3TA, United Kingdom

Received June 9, 1997; in revised form September 15, 1997; accepted September 19, 1997

Phase relations have been investigated within the $Sr_4Nb_4O_{14}$–$Sr_5Nb_4O_{15}$–$SrTiO_3$ region of the SrO–Nb_2O_5–TiO_2 system with a view to clarifying the occurrence of perovskite-related phases. Most samples were prepared from oxide or carbonate powders heated in air at 1350°C but some samples were also prepared by argon arc melting. Overall phase analysis was carried out by powder X-ray diffraction. Two phase lines contain a homologous series of layered perovskite phases. These are the $Sr_n(Nb,Ti)_nO_{3n+2}$ ($4 \le n \le 7$) series on the $Sr_4Nb_4O_{14}$–$SrTiO_3$ line and $Sr_n(Nb,Ti)_{n-1}O_{3n}$ ($5 \le n \le 7$) on the $Sr_5Nb_4O_{15}$–$SrTiO_3$ line. The microstructures in these homologous series were clarified by transmission electron microscopy. This revealed both ordered and disordered intergrowths of the perovskite homologues and allowed the defect microstructure of $SrTiO_3$ in contact with the layered perovskites to be determined.

INTRODUCTION

The SrO–Nb_2O_5–TiO_2 system contains a variety of interesting structure types, mainly constructed from different arrangements of transition metal–oxygen octahedra, with the large Sr^{2+} cations occupying tunnels or cages in this octahedral skeleton (1). Several phase regions, particularly those containing tetragonal tungsten bronze structures or perovskite structures, are of interest as dielectric or ferroelectric materials. Despite this interest, complete phase relations for the system are still lacking. In this paper we report results on a part of this phase region containing layered perovskite-related structures.

In general, this area is found in the SrO-rich part of the phase region. The prototype perovskite, $SrTiO_3$, is found at the midpoint of the TiO_2–SrO line on the phase diagram. Between $SrTiO_3$ and SrO a series of perovskite-related phases of the Ruddlesden–Popper type form (1, 2). These phases consist of slabs of perovskite structure cut along (100) and stacked so as to accommodate extra SrO at the interfaces. No other perovskite-related phases form on this line. Along the Nb_2O_5–SrO line the first phase that has recognizable perovskite-like regions is $SrNb_2O_6$(1) but these are linked by edge-shared octahedra and are rather different from the layered perovskite-related phases of interest here. The first simple layered perovskite encountered is $Sr_2Nb_2O_7$ (3). This phase consists of perovskite-like slabs cut along (110) and united so as to accommodate extra SrO in the interface (4) as shown in Fig. 1. The figure indicates that in this phase the perovskite slabs are four octahedra thick and a more correct designation of this structure, which we will use in this paper, is $Sr_4Nb_4O_{14}$. It corresponds to the $n = 4$ member of the homologous series of layered perovskite phases $A_nB_nO_{3n+2}$ in which the perovskite-like slabs are n octahedra thick. To the SrO-rich side of $Sr_4Nb_4O_{14}$ the phase $Sr_5Nb_4O_{15}$ is found (3). Although its exact structure has not yet been determined, it is certainly isostructural with $Ba_5Nb_4O_{15}$ (5) and is the $n = 5$ member of the $A_nB_{n-1}O_{3n}$ series of so-called hexagonal perovskites. In this structure slabs of normal cubic perovskite are intergrown with regions stacked in hexagonal close packing of the type found in the hexagonal perovskite $BaNiO_3$ as shown in Fig. 2. The change in composition from the ideal ABO_3 is brought about by layers of empty octahedra in the center of the hexagonal slabs, which would be filled with cations in the stoichiometric perovskite. The only other perovskite-related phase on the SrO–Nb_2O_5 tie line is $Sr_4Nb_2O_9$, which has been reported to have a disordered cubic perovskite structure, although one ordered variant has also been reported (6).

It is seen that the basic perovskite structure accommodates changes in composition in four different ways in the $Sr_4Nb_4O_{14}$–$SrTiO_3$–Sr_2TiO_4–$Sr_4Nb_2O_9$ quadrilateral region of the phase diagram. This paper goes some way to exploring this phase region and presents results on the phases and defect microstructures encountered, mainly determined via transmission electron microscopy and powder X-ray diffraction, for the $Sr_4Nb_4O_{14}$–$SrTiO_3$–$Sr_5Nb_4O_{15}$ triangle. Results on contiguous phase regions will be presented in the future.

EXPERIMENTAL

Samples on the composition lines $Sr_4Nb_4O_{14}$–$SrTiO_3$, $Sr_5Nb_4O_{15}$–$SrTiO_3$, and $Sr_4Nb_4O_{14}$–Sr_2TiO_4 were prepared using Specpure grade $SrCO_3$, Nb_2O_5, and TiO_2

0022-4596/98 $25.00

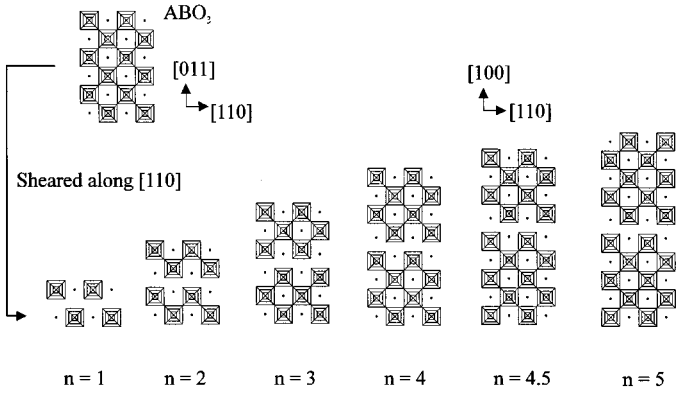

FIG. 1. Idealized structures of the series of layered perovskites $A_nB_nO_{3n+2}$ formed by stacking slabs of the perovskite structure in a regular sequence. The phase commonly referred to as $Sr_2Nb_2O_7$ is in fact the $n = 4$ member, $Sr_4Nb_4O_{14}$.

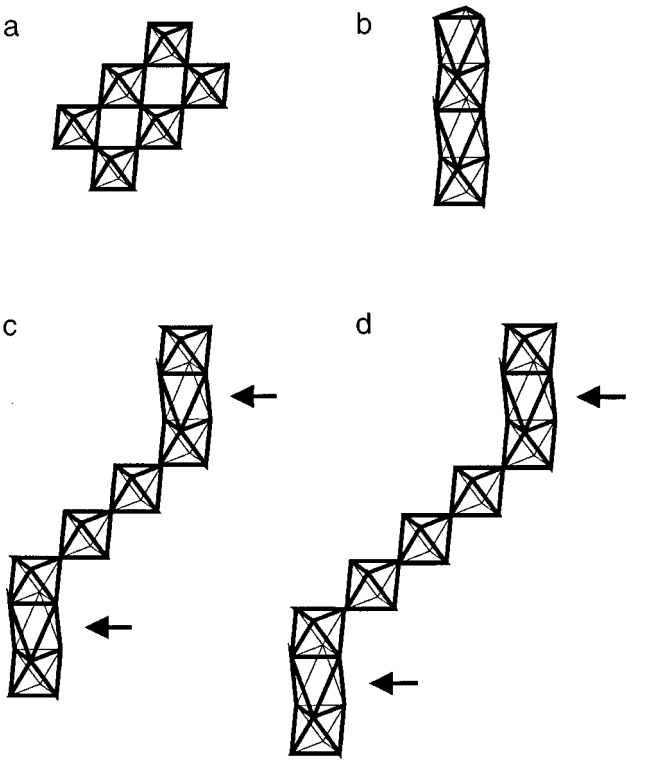

FIG. 2. Perspective views of the idealized structures of (a) the cubic perovskite structure, (b) the hexagonal perovskite structure found in $BaNiO_3$, (c) $Sr_5Nb_4O_{15}$, and (d) $Sr_6Nb_4TiO_{18}$. In (a) and (b) all octahedra are centered by transition metal cations whereas in (c) and (d) the octahedra in the center of the hexagonal slabs, arrowed, are empty, thus changing the composition from $A_nB_nO_{3n}$ to $A_nB_{n-1}O_{3n}$.

(Johnson Matthey). These chemicals were all dried at 110°C, and $SrCO_3$ was heated at 1000°C overnight to achieve decomposition to the oxide. Appropriate weights were then ground in an agate mortar and pressed into pellets. Samples on the composition lines $Sr_4Nb_4O_{14}$–$SrTiO_3$ and $Sr_4Nb_4O_{14}$–Sr_2TiO_4 were heated at 1200°C for 7 days. After regrinding, they were pressed again and heated at 1350°C for 3 days. Samples on the composition line $Sr_5Nb_4O_{15}$–$SrTiO_3$ were heated at 1400°C for 2 weeks, then at 1200°C for 3 days, and finally at 1200°C for 2 weeks. All samples were removed rapidly from the furnace and quenched into liquid nitrogen or iced brine. In addition, samples were ground and re-pressed between each heat treatment. Additionally, two samples of composition $Sr_6Nb_4TiO_{18}$ and $Sr_7Nb_4Ti_2O_{21}$ were prepared by arc-melting in argon as previously described (9).

X-ray powder diffraction data were obtained by using a Guinier–Hägg focusing camera (Expectron XDC-1000) with Cu$K\alpha_1$ radiation used as X-ray source and a Philips generator operating at 40 kV and 55 mA. X-ray powder patterns were indexed and refined using least squares methods.

Samples for transmission electron microscopy were prepared by crushing the pellets under 1-butanol and allowing a drop of the resultant suspension to dry on a copper grid coated with a holey carbon film. The transmission electron microscope used was a JEOL 200CX equipped with a LaB_6 filament operating at 200 kV and fitted with a top-entry goniometer stage.

RESULTS

Powder X-Ray Diffraction

$Sr_4Nb_4O_{14}$–$SrTiO_3$. The X-ray powder patterns indicated that this was a good tie line in the $Sr_4Nb_4O_{14}$–$SrTiO_3$–Sr_2TiO_4–$Sr_4Nb_2O_9$ quadrilateral as most films could, to a first approximation, be interpreted as containing only two phases, $Sr_4Nb_4O_{14}$ and $SrTiO_3$. The X-ray powder diagrams of the parent phases were indexed readily. For $Sr_4Nb_4O_{14}$ an orthorhombic cell of dimensions $a_0 = 0.3956$ nm, $b_0 = 2.680$ nm, and $c_0 = 0.5696$ nm was found, in good agreement with the literature values of $a_0 = 0.3955$ nm, $b_0 = 2.678$ nm, and $c_0 = 0.5701$ nm (4). The powder pattern of $SrTiO_3$ refined to yield a cubic cell of dimension $a_0 = 0.3902$ nm, which compares well with a literature value of 0.3905 nm (7).

X-ray powder patterns of the region between these two parent compounds showed a considerable amount of detail not described adequately in the preceding paragraph. In the composition region between $Sr_4Nb_4O_{14}$ and approximately 1 $Sr_4Nb_4O_{14}$: 3 $SrTiO_3$ a profusion of faint lines and diffuse reflections were apparent, all very close to lines from $Sr_4Nb_4O_{14}$. Despite the long preparation times employed, a sequence of sharp biphasic X-ray patterns could not be obtained and the patterns could not be cleanly indexed. However, the overall appearance of the films suggested that

layered perovskite phases similar to $Sr_4Nb_4O_{14}$ were present. Transmission electron microscopy was utilized to clarify the phases occurring in this composition range, as described later. Between the composition limits of $1\,Sr_4Nb_4O_{14}:3\,SrTiO_3$ and $SrTiO_3$, the layered perovskites coexisted with increasing amounts of $SrTiO_3$. Over this range the lattice parameters of $SrTiO_3$ remained constant and equal to that given in the preceding paragraph.

$Sr_4Nb_4O_{14}$–Sr_2TiO_4. Powder X-ray diffraction showed that this was not a good tie line in the $Sr_4Nb_4O_{14}$–$SrTiO_3$–Sr_2TiO_4–$Sr_4Nb_2O_9$ quadrilateral as the majority of films showed that three phases were present in each sample. The parent phase $Sr_4Nb_4O_{14}$ was found alone only at this exact composition. The X-ray powder data for this material were identical to those given in the preceding section. In compositions between $4.5\,Sr_4Nb_4O_{14}:1.0\,Sr_2TiO_4$ and $3.5\,Sr_4Nb_4O_{14}:3.0\,Sr_2TiO_4$, the powder patterns were similar to those on the $Sr_4Nb_4O_{14}$–$SrTiO_3$ line. The predominant phases present were layered perovskites. As with $Sr_4Nb_4O_{14}$–$SrTiO_3$, the complexity of the powder patterns did not allow individual phases to be identified apart from $Sr_4Nb_4O_{14}$. However, electron microscopy revealed that in this phase region layered perovskites related to $Sr_4Nb_4O_{14}$ were present, as described later. On all of these films the hexagonal perovskite phase $Sr_5Nb_4O_{15}$ was also recorded together with traces of $SrTiO_3$. At an overall composition of $3\,Sr_4Nb_4O_{14}:4\,Sr_2TiO_4$ lines from the layered perovskites were no longer present, confirming that the composition lay outside the triangle of interest here.

$Sr_5Nb_4O_{15}$–$SrTiO_3$. X-ray powder diffraction showed that this was a good tie line in the system as the powder patterns showed the presence of only one or two phases in each sample. The X-ray powder diffraction patterns from the pure phase $Sr_5Nb_4O_{15}$ were in agreement with the data of Carruthers and Grasso (3). These authors did not index their powder pattern and so we include the powder data in Table 1. The unit cell dimensions derived from these data were $a_0 = 0.5664$ nm and $c_0 = 1.148$ nm, which are in good agreement with the data for the isostructural phase $Ba_5Nb_4O_{15}$ (5), viz., $a_0 = 0.5794$ nm and $c_0 = 1.1784$ nm. A key to the identification of this structure type is the pair of strong lines at d values of approximately 0.300 and 0.283 nm. As the amount of $SrTiO_3$ in the samples increased, a number of new faint reflections appeared. However, it was the appearance of the strong doublet that was of most use for phase analysis. In these, the line at 0.300 nm broadened considerably toward lower d values whereas the line at 0.283 nm remained rather sharp. This latter line is a (110) line whereas the line at 0.300 nm is of the (101) type.

TABLE 1
Powder X-ray Diffraction Data for $Sr_5Nb_4O_{15}$[a]

hkl	d_{obs} (Å)	d_{calc} (Å)	Intensity
102	3.729	3.736	< 10
103	3.018	3.018	100
110	2.834	2.834	100
202	2.255	2.255	< 10
203	2.064	2.064	80
106	1.783	1.782	40
213	1.668	1.6611	60
300	1.635	1.637	40

[a] The refined unit cell has dimensions $a = 0.5664$ nm and $c = 1.148$ nm.

TABLE 2
Powder X-ray Diffraction Data for $Sr_6Nb_4TiO_{18}$[a]

hkl	d_{obs} (Å)	d_{calc} (Å)	Intensity
307	3.776	3.764	10
30 11	2.976	2.976	80
110	2.824	2.824	100
106	2.049	2.075	60
30 22	1.752	1.751	20
206?	1.658	1.672	30
300	1.630	1.630	40
108	1.624	1.621	30

[a] The refined unit cell has dimensions $a = 0.5648$ nm and $c = 1.3749$ nm.

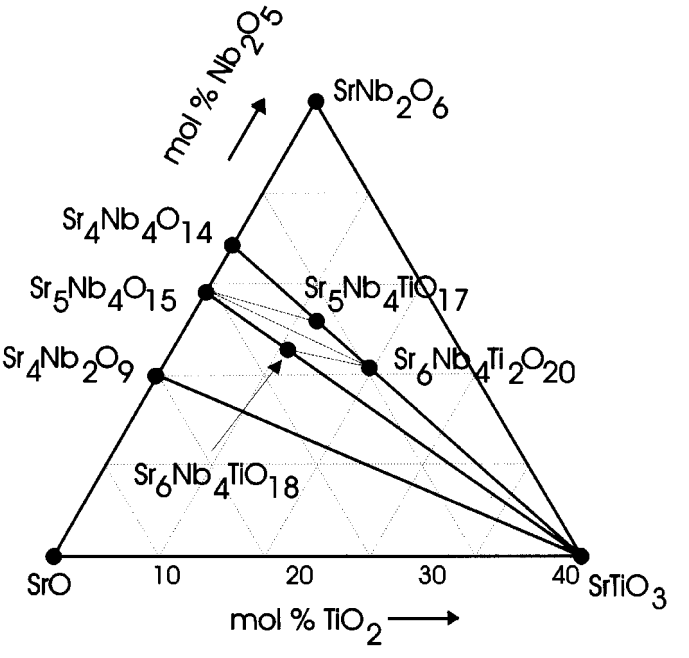

FIG. 3. Compatibility relations in the $Sr_4Nb_4O_{14}$–$SrTiO_3$–$Sr_5Nb_4O_{15}$ phase region.

Hence we interpreted this to show that a series of phases is occurring with *a* and *b* parameters very similar to those in $Sr_5Nb_4O_{15}$ but with considerable changes in the *c* parameter. This is consistent with the appearance of a homologous series of hexagonal perovskite phases along this tie line. Because of the disorder revealed in the powder patterns, the individual phases could not be separated in these samples but the interpretation was confirmed by electron microscopy, as described in the following section. Arc-melted samples provided sharper patterns and showed that the new hexagonal perovskite phase $Sr_6Nb_4TiO_{18}$ coexisted with $SrTiO_3$ along the tie line in samples quenched from the melt. The indexed powder pattern of $Sr_6Nb_4TiO_{18}$ is given in Table 2. The lattice parameters derived from these data are $a_0 = 0.5648$ nm and $c_0 = 1.3749$ nm. The lattice parameter of the $SrTiO_3$ was identical to that reported earlier.

The foregoing information, supplemented by the following electron microscopy results, allowed the phase relations shown in Fig. 3 to be determined.

Transmission Electron Microscopy

$Sr_4Nb_4O_{14}$–$SrTiO_3$. Transmission electron microscopy showed that for compositions near to $Sr_4Nb_4O_{14}$ the material consisted of slightly disordered crystals. $Sr_4Nb_4O_{14}$ corresponds to the $n = 4$ member of the homologous series $Sr_nNb_nO_{3n+2}$ and the disorder consisted of interpolated slabs of perovskite structure that had a thickness appropriate to the $n = 5$ phase, $Sr_5Nb_4TiO_{17}$. These wider slabs were generally distributed randomly throughout the structure and the frequency increased relative to the $n = 4$ slabs as the composition moved away from $Sr_4Nb_4O_{14}$. Ultimately, crystal fragments of the $n = 5$ phase $Sr_5Nb_4TiO_{17}$ predominated. Further addition of $SrTiO_3$ repeated this type of structural evolution, with slabs corresponding to the $n = 6$ phase $Sr_6Nb_4Ti_2O_{20}$ growing into an $n = 5$ $Sr_5Nb_4TiO_{17}$ matrix with an increasing frequency until pure fragments of the $n = 6$ structure were found. No other members of the homologous series were found in a pure form but crystal fragments largely containing the $n = 7$ phase $Sr_7Nb_4Ti_3O_{23}$ were occasionally located. Electron micrographs of materials similar to these layered perovskites have recently been found in the $Nd_4Ti_4O_{14}$–$SrTiO_3$ (8,9), $Nd_4Ti_4O_{14}$–$NdTiO_3$ (10), and related systems (11–13) and it is unnecessary to show almost identical micrographs here.

Samples containing increasing quantities of $SrTiO_3$ generally consisted of regions of the $n = 6$ material

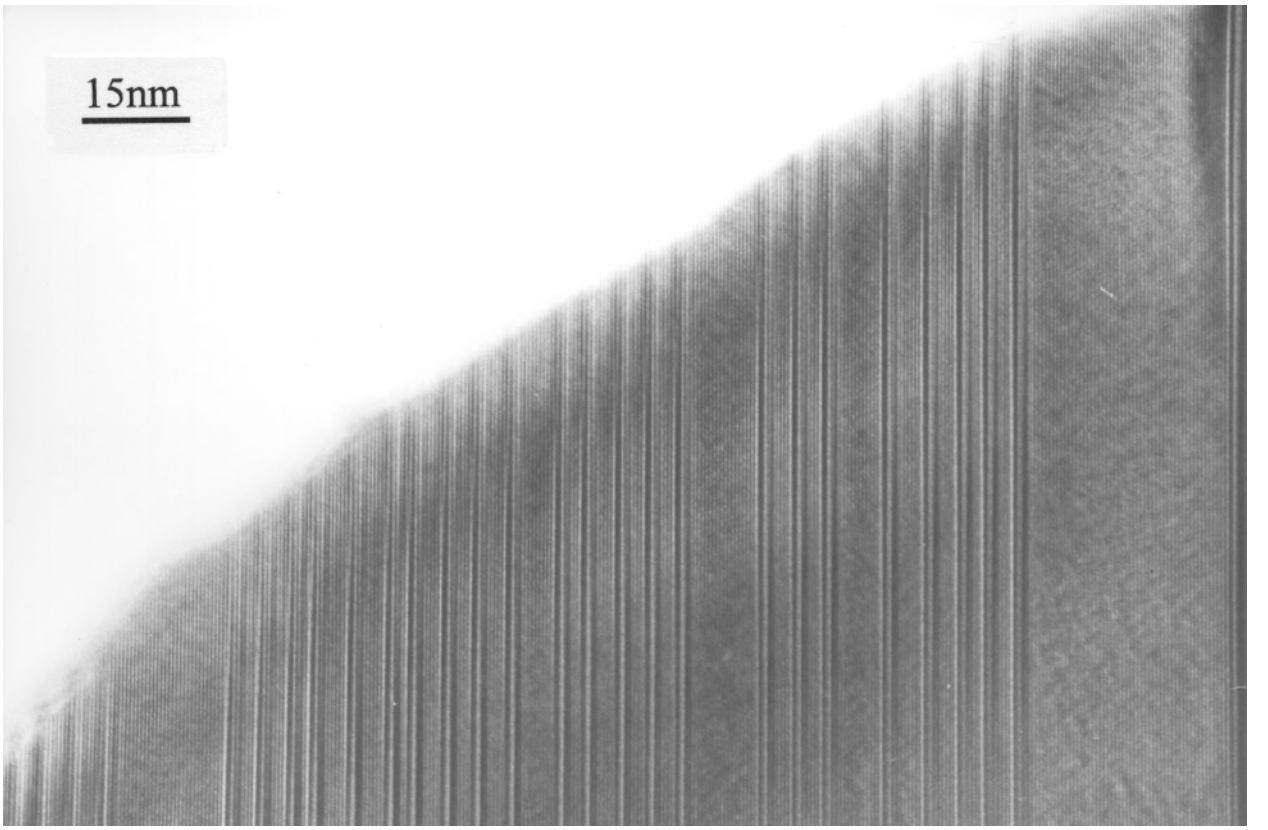

FIG. 4. Electron micrograph showing a disordered layered perovskite material containing wider slabs of $SrTiO_3$. The boundaries lie along [110] with respect to the perovskite parent structure as shown in Fig. 1.

$Sr_6Nb_4Ti_2O_{20}$ interspersed with slabs or wider regions corresponding to the $n = 7$ homologue $Sr_7Nb_4Ti_3O_{23}$ and wider perovskite-like ($SrTiO_3$) regions of very varied thickness. Such a fragment is shown in Fig. 4. The interface between the layered perovskite region and the $SrTiO_3$ region corresponded to (010) planes with respect to the layered phase. Occasionally, the interfaces between the layered perovskite region and the $SrTiO_3$ region did not extend completely through the crystal fragment. Under these circumstances the layered slabs terminated in hairpin-like arrangements as shown in Fig. 5.

At increasing concentrations of $SrTiO_3$ the presence of layered structures decreased and became more difficult to locate. The $SrTiO_3$ fragments located showed no significant defect structure and have not been illustrated.

$Sr_4Nb_4O_{14}$–Sr_2TiO_4 close to $Sr_4Nb_4O_{14}$. As would be expected from the phase diagram shown in Fig. 2, the microstructures found in these samples were disordered layered perovskites identical to those already described together with well-ordered fragments of the hexagonal perovskite $Sr_5Nb_4O_{15}$. Because this composition line is not a true tie line, little effort was put into determining the exact phase range of the materials as the main purpose of the study was to ascertain whether the tie lines were from $Sr_4Nb_4O_{14}$ to the hexagonal perovskites or from $Sr_5Nb_4O_{15}$ to the

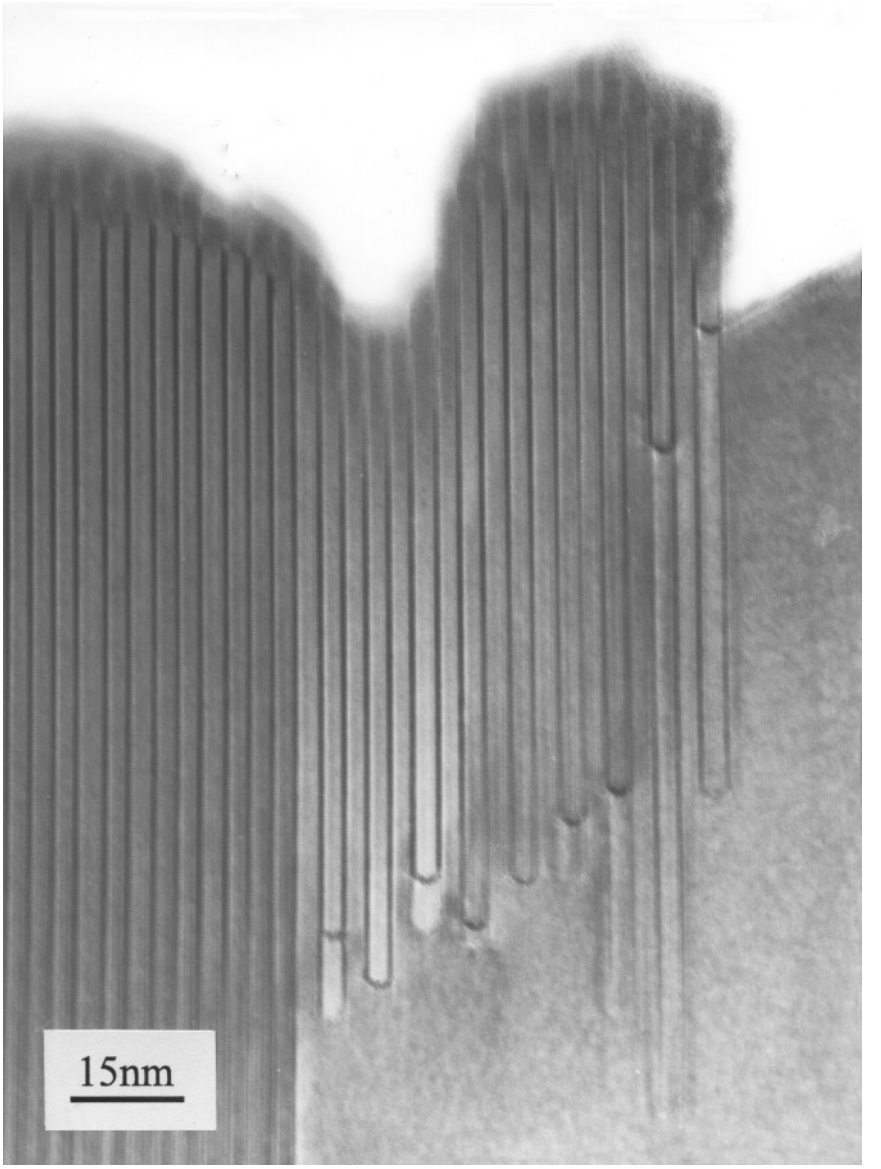

FIG. 5. Electron micrograph showing hairpin-type terminations of slabs of layered perovskite material coexisting with $SrTiO_3$. The boundaries lie along [110] with respect to the perovskite parent structure as shown in Fig. 1.

layered perovskites, as drawn. No crystal fragments were found in which a layered perovskite region coexisted with a hexagonal perovskite region.

$Sr_5Nb_4O_{15}$–$SrTiO_3$. In the present study well-ordered crystals of $Sr_5Nb_4O_{15}$, the $n = 5$ member of the homologous series, were encountered frequently. A typical example of this material is shown in Fig. 6, which shows the stacking perpendicular to the *c*-axis. In addition, sporadic evidence for additional ordering in the hexagonal *a*–*b* plane was provided by the occasional presence of faint superstructure reflections on some diffraction patterns.

As the overall composition of the samples moved toward $SrTiO_3$, random or partly ordered intergrowths of slabs corresponding to the previously unreported $n = 6$ homologue, $Sr_6Nb_4TiO_{18}$, appeared as illustrated in Fig. 7. In addition to disordered fragments, we found well-ordered crystals corresponding to a 1:1 order of these slabs to generate the compound $Sr_{11}Nb_8TiO_{33}$, which is the 5.5 homologue in the series. As the $SrTiO_3$ concentration increased, the phase $Sr_6Nb_4TiO_{18}$ was ultimately found alone, the micrographs being very similar in appearance to Fig. 6. At still greater concentrations of $SrTiO_3$, slabs of hexagonal perovskite structure equivalent to the $n = 7$ homologue, $Sr_7Nb_4Ti_2O_{21}$, began to appear and eventually this phase dominated. Crystal fragments in which the $n = 7$ phase contained wider $n = 8$ slabs were also found, as shown in Fig. 8. However, these crystals were rare and more often hexagonal perovskites with $n = 6$ or higher coexisted with $SrTiO_3$, as shown in Fig. 9. From this figure it is apparent that the interface between these two regions is (001) with respect to the hexagonal structure, which is to be expected from a crystallographic point of view.

DISCUSSION

The results presented have clarified the phase diagram in the phase region $Sr_4Nb_4O_{14}$–$Sr_5Nb_4O_{15}$–$SrTiO_3$. The existence triangle shown in Fig. 3 refers to the situation for samples prepared at temperatures of 1350°C or above. On the $Sr_4Nb_4O_{14}$–$SrTiO_3$ phase lines a homologous series of perovskite-related structures $Sr_nB_nO_{3n+2}$ occurs with the $n = 6$ or 7 phases in equilibrium with the perovskite $SrTiO_3$. On moving into the $Sr_4Nb_4O_{14}$–$Sr_5Nb_4O_{15}$–

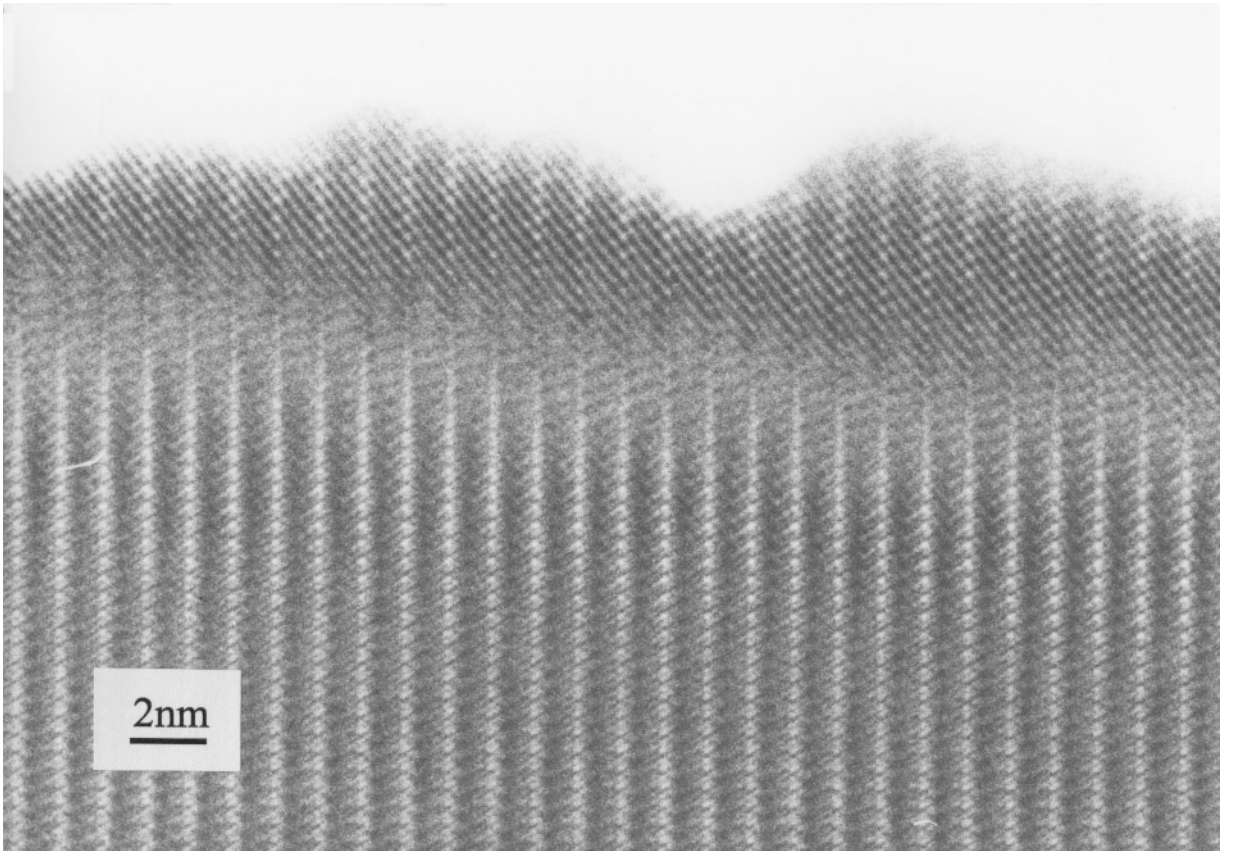

FIG. 6. Electron micrograph showing a well-ordered fragment of the hexagonal perovskite $Sr_5Nb_4O_{15}$. The boundaries running vertically in the micrograph are normal to the hexagonal *c*-axis.

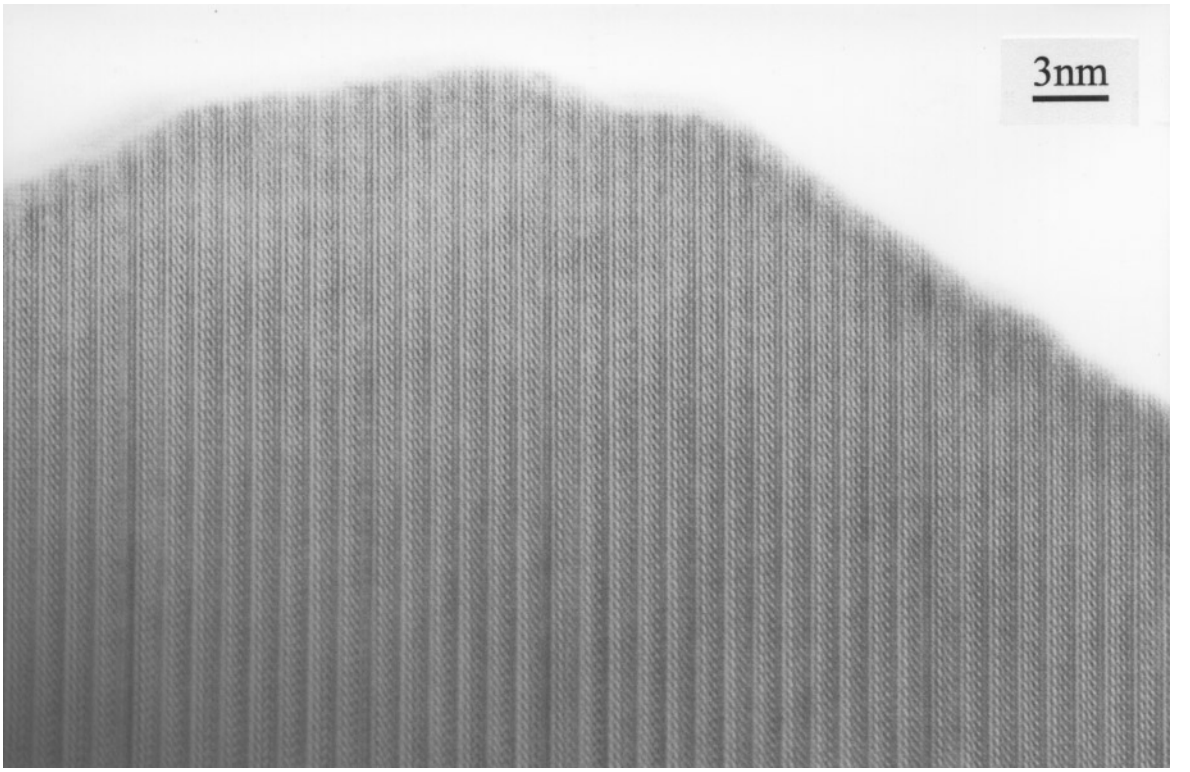

FIG. 7. Electron micrograph of a disordered fragment of the hexagonal perovskite phase $Sr_5Nb_4O_{15}$. The disorder consists of wider slabs of structure equivalent to the phase $Sr_6Nb_4TiO_{18}$. The boundaries running vertically in the micrograph are normal to the hexagonal *c*-axis.

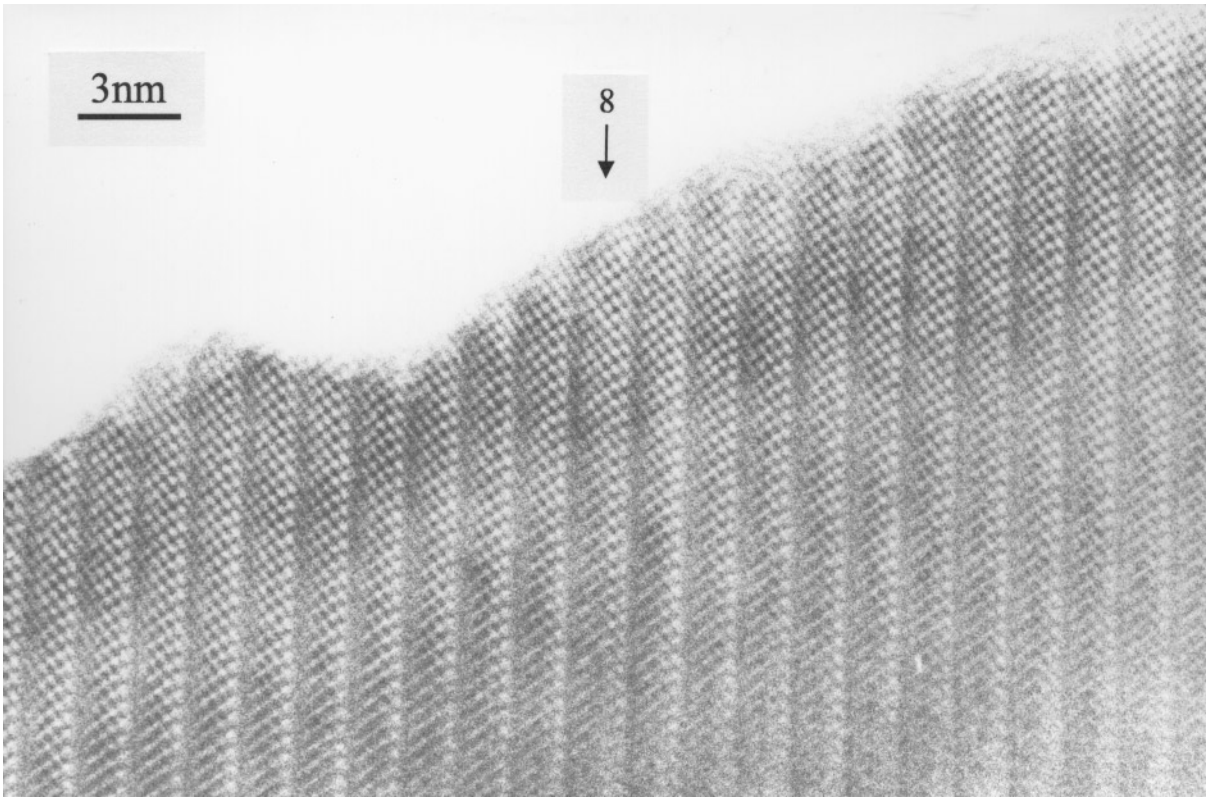

FIG. 8. Electron micrograph of a fragment of a crystal of $Sr_7Nb_4Ti_2O_{21}$ containing a single lamella of width equivalent to the phase $Sr_8Nb_4Ti_3O_{24}$. The boundaries running vertically in the micrograph are normal to the hexagonal *c*-axis.

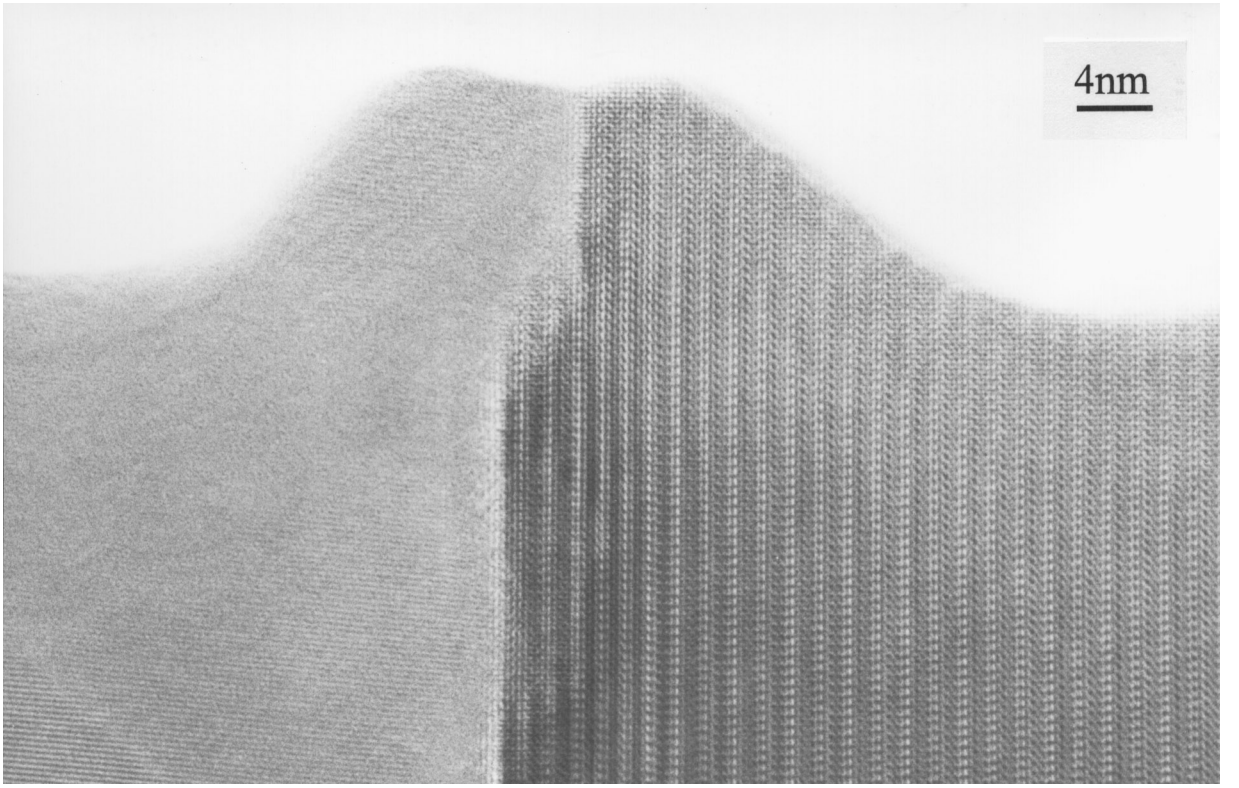

FIG. 9. Electron micrograph showing the hexagonal perovskite phase $Sr_6Nb_4TiO_{18}$ coexisting with $SrTiO_3$. The boundaries running vertically in the micrograph are normal to the hexagonal *c*-axis.

$SrTiO_3$ triangle, these phases coexist with $Sr_5Nb_4O_{15}$. The phase lines joining $Sr_5Nb_4O_{15}$ to these homologues are drawn as dotted lines because in ceramic samples exact phase equilibria were not achieved. However, given sufficiently careful preparation and long enough annealing, this series of existence triangles should be found. On the $Sr_5Nb_4O_{15}$–$SrTiO_3$ line another homologous series is found, $A_nB_{n-1}O_{3n}$, again with the $n = 6$ or 7 phases in equilibrium with the perovskite $SrTiO_3$. These phases coexist with $SrTiO_3$ in the $SrTiO_3$–$Sr_5Nb_4O_{15}$–$Sr_7Nb_4Ti_2O_{21}$ existence triangle. Again, long heating times and careful preparation would be necessary to obtain true existence triangles as shown in Fig. 3. In addition, the actual homologue in equilibrium with $SrTiO_3$ is expected to vary with temperature and at lower temperatures it is unlikely that the higher homologues will form. For example, on the $Sr_4Nb_4O_{14}$–$SrTiO_3$ line, only $Sr_4Nb_4O_{14}$ is found at 1250°C. The diagram must therefore be interpreted with some degree of caution.

In terms of the details of the phase region, a number of previously unreported layered perovskite phases were characterized. On the $Sr_4Nb_4O_{14}$–$SrTiO_3$ line we have characterized with confidence $Sr_5Nb_4TiO_{17}$ and $Sr_6Nb_4Ti_2O_{20}$, the $n = 5$ and $n = 6$ members of the homologous series, in which the perovskite-like slabs are respectively 5 and 6 octahedra wide. It is also clear that the $n = 7$ member, $Sr_7Nb_4Ti_3O_{23}$, is also present in small quantities. Between these phases a variety of ordered and disordered distribution of slabs of thickness equivalent to those in the $n = 4$ and 5, $n = 5$ and 6, and $n = 6$ and 7 structures were recorded. This is normal in these types of systems and explains why the resolution of the system by powder X-ray diffraction is difficult. Although the $n = 7$ compound $Sr_7Nb_4Ti_3O_{21}$ was found, in our specimens this phase always seemed to be rather disordered. The disorder took the form of slabs equivalent to the $n = 6$ phase and at other times wider slabs were also encountered. As the composition approached $SrTiO_3$, these slabs became wider and wider. Although in a formal sense it is possible to refer to these as lamellae of phases with n equivalent to 10 or more, this seems to be an inaccurate way of describing the situation. It is more reasonable to suggest that the $n = 7$ structure more or less coexists with $SrTiO_3$-like regions.

The $Sr_5Nb_4O_{15}$–$SrTiO_3$ tie line seems to behave in a similar fashion. The parent phase is the hexagonal perovskite $Sr_5Nb_4O_{15}$, with a structure that consists of layers of hexagonal stacking separated by a slab of cubic material. In the present study we have found well-ordered examples of

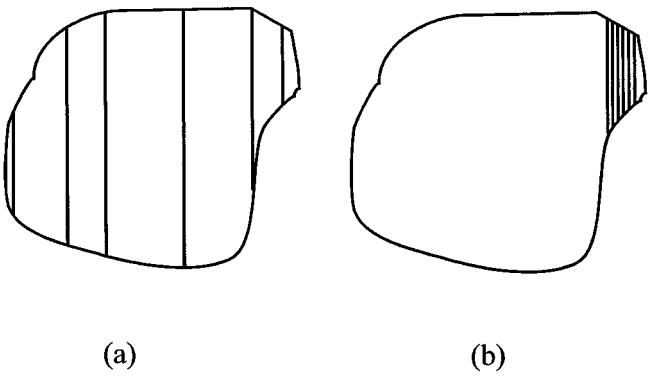

FIG. 10. Schematic illustration of the microstructure of crystals in equilibrium with $SrTiO_3$. The situation that prevails is closer to that shown in (b) rather than (a).

the next two phases in the series, $Sr_6Nb_4TiO_{18}$ and $Sr_7Nb_4Ti_2O_{21}$, the $n = 6$ and 7 compounds, and fragments containing well-ordered lamellae of the $n = 5$ and $n = 6$ phases corresponding to the compound $Sr_{11}Nb_8TiO_{33}$, which is the 5.5 homologue in the series. Similar ordered fragments may well be found in the region between $n = 6$ and $n = 7$ if sought.

In each of the series of phases found the equilibrium between the complex phases and $SrTiO_3$ took on a similar form. Regions of crystal containing high-n material become disordered by the incorporation of wider slabs of $SrTiO_3$. This indicates the general structure of these intermediate compositions is given rather more by the situation illustrated in Fig. 10b than that in Fig. 10a. The boundary between the layered phase and the $SrTiO_3$ matrix tends to be identical to the cubic perovskite slab boundaries. Thus the $Sr_4Nb_4O_{14}$ series joins along (010) planes and the $Sr_5Nb_4O_{15}$ series joins along (001) planes. When a layered perovskite phase coexists with $SrTiO_3$ along a crystallographic plane other than these, the terminations seem to link up in a hairpin arrangement. This is probably to minimize strain energy and could well reflect the mechanism by which these lamellae grow or shrink in the $SrTiO_3$ matrix.

Although the studies outlined herein have made some aspects of the phase diagram clear, there are still some questions outstanding. In particular, it is of interest to relate these findings to the phase equilibria pertaining at lower temperatures and in the other regions of the $Sr_4Nb_4O_{14}$–$SrTiO_3$–Sr_2TiO_4–$Sr_4Nb_2O_9$ quadrilateral. Studies are underway to clarify these issues and will be published in the future.

ACKNOWLEDGMENT

D.P. is grateful to the CEC (Contract No. CT93.3057) for financial support during a part of this study.

REFERENCES

1. B. G. Hyde and S. Andersson, "Inorganic Crystal Structures." Wiley-Interscience, New York, 1989.
2. R. J. D. Tilley, *J. Solid State Chem.* **21,** 293 (1977).
3. J. R. Carruthers and M. Grasso, *J. Electrochem. Soc.* **117,** 1426 (1970).
4. N. Ishizawa, F. Narumo, T. Kawamura, and M. Kimura, *Acta Crystallogr, Sect. B: Struct. Crystallogr. Cryst. Chem.* **B31,** 1912 (1975).
5. R. S. Roth and J. L. Waring, *J. Res. Natl. Bur. Stand., Sect. A* **65A,** 337 (1961).
6. M. Hervieu, B. Raveau, J. Lecomte, and L. J. Loup, *Chem. Scr.* **25,** 206 (1985).
7. H. Swanson, *Natl. Bull. Stand. Circ. (U.S.)* **No. 539,** 3, 44 (1959).
8. J. Sloan and R. J. D. Tilley, *J. Solid State Chem.* **121,** 324 (1996).
9. J. Sloan and R. J. D. Tilley, *Eur. J. Solid State Inorg. Chem.* **31,** 673 (1996).
10. E. Connolly, J. Sloan, and R. J. D. Tilley, *Eur. J. Solid State Inorg. Chem.* **33,** 371 (1996).
11. T. B. Williams, F. Lichtenberg, D. Widmer, J. G. Bednorz, and A. Reller, *J. Solid State Chem.* **93,** 534 (1991).
12. F. Lichtenberg, T. B. Williams, A. Reller, D. Widmer, and J. G. Bednorz, *Z. Phys. B* **84,** 369 (1991).
13. T. B. Williams, F. Lichtenberg, D. Widmer, J. G. Bednorz, and A. Reller, *J. Solid State Chem.* **103,** 375 (1991).